

A Search for Warm/Hot Gas Filaments Between Pairs of SDSS Luminous Red Galaxies

Hideki Tanimura,¹★ Gary Hinshaw,^{1,2,3} Ian G. McCarthy,⁴ Ludovic Van Waerbeke,^{1,2} Yin-Zhe Ma,⁵ Alexander Mead,¹ Alireza Hojjati¹ and Tilman Tröster¹

¹*Department of Physics and Astronomy, University of British Columbia, Vancouver, BC V6T 1Z1, Canada*

²*Canadian Institute for Advanced Research, 180 Dundas St W, Toronto, ON M5G 1Z8, Canada*

³*Canada Research Chair in Observational Cosmology*

⁴*Astrophysics Research Institute, Liverpool John Moores University, Liverpool, L3 5RF, United Kingdom*

⁵*Astrophysics and Cosmology Research Unit, School of Chemistry and Physics, University of KwaZulu-Natal, Durban, South Africa*

16 September 2021

ABSTRACT

We search the *Planck* data for a thermal Sunyaev-Zel’dovich (tSZ) signal due to gas filaments between pairs of Luminous Red Galaxies (LRG’s) taken from the Sloan Digital Sky Survey Data Release 12 (SDSS/DR12). We identify $\sim 260,000$ LRG pairs in the DR12 catalog that lie within $6\text{--}10\ h^{-1}\text{Mpc}$ of each other in tangential direction and within $6\ h^{-1}\text{Mpc}$ in radial direction. We stack pairs by rotating and scaling the angular positions of each LRG so they lie on a common reference frame, then we subtract a circularly symmetric halo from each member of the pair to search for a residual signal between the pair members. We find a statistically significant (5.3σ) signal between LRG pairs in the stacked data with a magnitude $\Delta y = (1.31 \pm 0.25) \times 10^{-8}$. The uncertainty is estimated from two Monte Carlo null tests which also establish the reliability of our analysis. Assuming a simple, isothermal, cylindrical filament model of electron over-density with a radial density profile proportional to r_c/r (as determined from simulations), where r is the perpendicular distance from the cylinder axis and r_c is the core radius of the density profile, we constrain the product of over-density and filament temperature to be $\delta_c \times (T_e/10^7\text{ K}) \times (r_c/0.5h^{-1}\text{ Mpc}) = 2.7 \pm 0.5$. To our knowledge, this is the first detection of filamentary gas at over-densities typical of cosmological large-scale structure. We compare our result to the BAHAMAS suite of cosmological hydrodynamic simulations (McCarthy et al. 2017) and find a slightly lower, but marginally consistent Comptonization excess, $\Delta y = (0.84 \pm 0.24) \times 10^{-8}$.

Key words: galaxies – groups – clusters – halos – filaments – large-scale structure – cosmology

1 INTRODUCTION

In the now-standard Λ CDM cosmology, more than 95% of the energy density in the universe is in the form of dark matter and dark energy, whereas baryonic matter only comprises 4.6% (Planck Collaboration et al. 2016a; Hinshaw et al. 2013).

At high redshift ($z \gtrsim 2$), most of the expected baryons are found in the Ly α absorption forest: the diffuse, photo-ionized intergalactic medium (IGM) with a temperature of $10^4\text{--}10^5\text{ K}$ (e.g., Weinberg et al. 1997; Rauch et al. 1997). However, at redshifts $z \lesssim 2$, the observed baryons in stars, the cold interstellar medium, residual Ly α forest gas, OVI and BLA absorbers, and hot gas in clusters of galaxies account for only $\sim 50\%$ of the expected baryons – the remainder has yet to be identified (e.g., Fukugita & Peebles

2004; Nicastro et al. 2008; Shull et al. 2012). Hydrodynamical simulations suggest that 40–50% of baryons could be in the form of shock-heated gas in a cosmic web between clusters of galaxies. This so-called Warm Hot Intergalactic Medium (WHIM) has a temperature range of $10^5\text{--}10^7\text{ K}$ (Cen & Ostriker 2006). The WHIM is difficult to observe due to its low density: several detections in the far-UV and X-ray have been reported, but none are considered definitive (Yao et al. 2012).

The thermal Sunyaev-Zel’dovich (tSZ) effect (Zeldovich & Sunyaev 1969; Sunyaev & Zeldovich 1970, 1972, 1980) arises from the Compton scattering of CMB photons as they pass through hot ionized gas along the line of sight. The signal provides an excellent tool for probing baryonic gas at low and intermediate redshifts. Atrio-Barandela & Mücke (2006) and Atrio-Barandela et al. (2008) suggest that electron pressure in the WHIM would be sufficient to generate potentially observable tSZ signals. However, the

★ E-mail: tanimura@phas.ubc.ca

measurement is challenging due to the morphology of the source and the relative weakness of the signal.

The *Planck* satellite mission has produced a full-sky tSZ map with 10 arcmin angular resolution and high sensitivity. In addition to the numerous galaxy clusters detected in tSZ by *Planck*, the *Planck* team reports a significant tSZ signal in the inter-cluster region between the merging clusters of A399–A401 (Planck Collaboration et al. 2013b). In conjunction with ROSAT X-ray data, they estimate the temperature and density of the inter-cluster gas to be $kT = 7.1 \pm 0.9$ keV with a baryon density of $(3.7 \pm 0.2) \times 10^{-4} \text{ cm}^{-3}$.

On a larger scale, luminous red galaxies (LRG's) are powerful tracers of large-scale structure of the universe. These early-type, massive galaxies, selected on the basis of color and magnitude, consist mainly of old stars with little ongoing star formation. LRG's typically reside in the centers of galaxy groups and clusters and have been used to detect and characterize the remnants of baryon acoustic oscillations (BAO) at low to intermediate redshift (Eisenstein et al. 2005; Kazin et al. 2010; Anderson et al. 2014).

Clampitt et al. (2016) searched for evidence of massive filaments between proximate pairs of LRG's taken from the Sloan Digital Sky Survey seventh data release (SDSS DR7). Using weak gravitational lensing signal, stacked on 135,000 pairs of LRG's, they find evidence for filament mass at $\sim 4.5\sigma$ confidence. Similarly, Epps & Hudson (2017) detect the weak lensing signal using the Canada France Hawaii Telescope Lensing Survey (CFHTLenS) mass map from stacked filaments between SDSS-III/BOSS LRG's at 5σ confidence.

Van Waerbeke et al. (2014), Ma et al. (2015) and Hojjati et al. (2015) report correlations between gravitational lensing and tSZ signals in the field using the CFHTLenS mass map and *Planck* tSZ map. Similarly, Hill & Spergel (2014) reports a statistically significant correlation between the *Planck* CMB lensing potential and the *Planck* tSZ map. These results show clear evidence for diffuse gas tracing dark matter. Further, in the context of a halo model, there is clear evidence for contributions from both the one- and two-halo terms, but there is no statistically significant evidence for contributions from diffuse, unbound gas not associated with (correlated) collapsed halos.

In this paper, we use the *Planck* tSZ map from the 2015 data release (Planck Collaboration et al. 2016a) to search for evidence of hot gas in filaments between proximate pairs of LRG's taken from the Sloan Digital Sky Survey twelfth data release (Alam et al. 2015): SDSS DR12 LRG (Prakash et al. 2016). Since the signal-to-noise ratio of the *Planck* y map is not high enough to trace individual filaments on this scale, we employ a stacking method to search for an average signal between many pairs. We find a mean filament signal of $\Delta y = (1.31 \pm 0.25) \times 10^{-8}$ with 5.3σ significance. We compare the filament signal with predictions from the BAHAMAS suite of hydrodynamic simulations (McCarthy et al. 2017) and find marginally consistent results for two cosmologies (WMAP9 and *Planck* 2013) in the suite. Throughout this work, we adopt a Λ CDM cosmology with $\Omega_m = 0.3$, $\Omega_\Lambda = 0.7$, and $H_0 = 70 \text{ km s}^{-1} \text{ Mpc}^{-1}$ for conversion of redshifts into distances.

2 DATA

We use three data sets in this analysis: 1) the Luminous Red Galaxy catalog from the Sloan Digital Sky Survey twelfth data release¹

(SDSS DR12 LRG, $N \sim 1,400,000$, Prakash et al. (2016)), 2) the *Planck* Comptonization y map² from the 2015 data release (Planck Collaboration et al. 2016a), and 3) the BAHAMAS suite of cosmological hydrodynamic simulations (McCarthy et al. 2017). We describe each briefly, in turn.

2.1 LRG pair catalog

SDSS Data Release 12 (DR12) is the final release of data from SDSS-III. The catalog provides the position, spectroscopic redshift, and classification type for each object. We extract objects identified as `sourceType=LRG`. The stellar masses of these objects have been estimated by three different groups³. We use the estimate based on a principal component analysis method by Chen et al. (2012), which uses stellar evolution synthesis models from Bruzual & Charlot (2003), and a stellar initial mass function from Kroupa (2001). For the stacking analysis, we select LRG's with $M_* > 10^{11.3} M_\odot$. According to the M_* – Y_{500} scaling relation reported in Planck Collaboration et al. (2013c) (Y_{500} is the Comptonization parameter integrated over a sphere of radius R_{500}), these LRG's should have a central tSZ signal-to-noise ratio of order unity. Since our analysis requires us to estimate and subtract the tSZ signal associated with the halos of the individual LRG's, this cut enhances the reliability of that estimation, via the procedure described in §3.2.

Not all LRG's are central galaxies in massive halos. Hoshino et al. (2015) find that, at a halo mass of $10^{14.5} M_\odot$, only 73% of LRG's are central, lower than the previous estimate of 89% obtained from correlation studies (Reid & Spergel 2009). To minimize the fraction of satellite LRG's in our sample (which could bias a filament signal) we select the locally most-massive LRG's (based on stellar mass) using a criterion that is analogous to that used in Planck Collaboration et al. (2013c): we reject a given galaxy if a more massive galaxy resides within a tangential distance of $1.0 h^{-1} \text{ Mpc}$ and within a radial velocity difference of $|c\Delta z| < 1000 \text{ km s}^{-1}$.

We construct the LRG pair catalog from this central LRG catalog by finding all neighbouring LRG's within a tangential distance of $6\text{--}10 h^{-1} \text{ Mpc}$ and within a proper radial distance of $\pm 6 h^{-1} \text{ Mpc}$. The resulting catalog has 262,864 LRG pairs to redshifts $z \sim 0.4$. Their redshift and separation distributions are shown in Figure 1.

2.2 Planck y map

The *Planck* tSZ map is one of the datasets provided in the *Planck* 2015 data release. It is available in HEALpix⁴ format with a pixel resolution of $N_{\text{side}} = 2048$. Two types of y map are publicly available: MILCA and NILC, both of which are based on multi-band combinations of the *Planck* band maps (Planck Collaboration et al. 2016b). Our analysis is based on the MILCA map, but we obtain consistent results with the NILC map.

The 2015 data release also provides sky masks suitable for analyzing the y maps, including a point source mask and galactic masks that exclude 40, 50, 60 and 70% of the sky. We combine the point source mask with the 40% galactic mask which excludes $\sim 50\%$ of the sky. The mask is applied during the stacking process:

² <http://pla.esac.esa.int/pla/#results>

³ <http://www.sdss.org/dr12/spectro/galaxy>

⁴ <http://healpix.sourceforge.net/>

¹ http://www.sdss.org/dr12/spectro/spectro_access

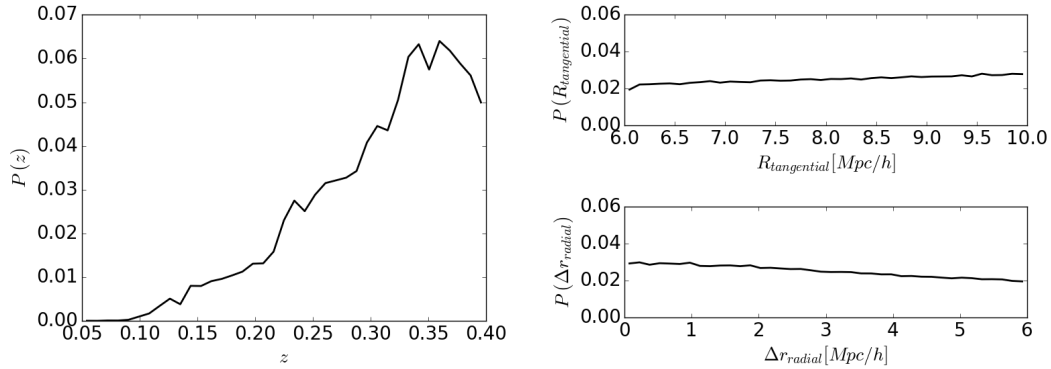


Figure 1. *Left:* The redshift distribution of LRG pairs peaks at $z \sim 0.35$. *Top right:* The distribution of tangential separations between LRG pairs. *Bottom right:* The distribution of radial separations between LRG pairs.

for a given LRG pair, masked pixels in the y map near that pair are not accumulated in the stacked image.

2.3 Simulations

To compare our results with theory, we analyze the BAHAMAS suite of cosmological smoothed particle hydrodynamics (SPH) simulations (McCarthy et al. 2017) in the same manner as the data. The BAHAMAS suite is a direct descendant of the OWLS (Schaye et al. 2010) and cosmo-OWLS projects (Le Brun et al. 2014; van Daalen et al. 2014; McCarthy et al. 2014). The simulations reproduce a variety of observed gas features in groups and clusters of galaxies in the optical and X-ray bands. The BAHAMAS suite consists of periodic box hydrodynamical simulations, the largest of which have volumes of $(400 h^{-1} \text{Mpc})^3$ and contain 1024^3 each of baryonic and dark matter particles. The suite employs two different cosmological models: the WMAP9 cosmology (Hinshaw et al. 2013) with

$$\{\Omega_m, \Omega_b, \Omega_\Lambda, \sigma_8, n_s, h\} = \{0.2793, 0.0463, 0.7207, 0.821, 0.972, 0.700\},$$

and the Planck 2013 cosmology (Planck Collaboration et al. 2014) with

$$\{\Omega_m, \Omega_b, \Omega_\Lambda, \sigma_8, n_s, h\} = \{0.3175, 0.0490, 0.6825, 0.834, 0.9624, 0.6711\}.$$

We have four realizations based on the WMAP9 cosmology and one based on the Planck 2013 cosmology.

From each realization, 10 nearly-independent mock galaxy catalogues are generated on 10 nearly-independent light cones, and 10 corresponding y maps are generated from the hot gas component of the simulation (McCarthy et al. 2014). Each of the light cones contain about one million galaxies out to $z \sim 1$, and each spans a $10^\circ \times 10^\circ$ patch of sky. To compare with data, we convolve the simulated y maps with a Gaussian kernel of 10 arcmin, FWHM, corresponding to the Planck beam.

3 DATA ANALYSIS

In this section we describe our procedure for stacking a y map against LRG pairs, we estimate and subtract the signal associated with single galaxy haloes, and we estimate the uncertainty of our final result.

3.1 Stacking on LRG pairs

The angular separation between LRG pairs in our catalog ranges between 27 and 203 arcmin. For each pair in the catalog, we follow Clampitt et al. (2016) and form a normalized 2-dimensional image coordinate system, (X, Y) , with one LRG placed at $(-1, 0)$ and the other placed at $(+1, 0)$. The corresponding transformation from sky coordinates to image coordinates is also applied to the y map and the average is taken over all members in the catalog. The mean tSZ signal in the annular region $9 < r < 10$ ($r^2 = X^2 + Y^2$) is subtracted as an estimate of the local background signal.

The top panel of Figure 2 shows the average y map stacked against 262,864 LRG pairs over the domain $-3 < X, Y < +3$, and the lower panel shows a slice of this map at $Y = 0$. Not surprisingly, the average signal is dominated by the halo gas associated with the individual LRGs in each pair. The peak amplitude of this signal is $\Delta y \sim 1.2 \times 10^{-7}$.

3.2 Subtracting the halo contribution

We estimate the average contribution from single LRG halos as follows. Since we have selected central LRGs for our pair catalog, we assume that the average single-halo contribution is circularly symmetric about each LRG in a pair. To determine the radial profile of each single halo, we fit the map (indexed by pixel p) to a model of the form

$$y_h(p) = y_{L,i}(p) + y_{R,j}(p), \quad (1)$$

where $y_{L,i}$ is the single-halo signal in the i th radial bin centred on the “left” LRG at $(-1, 0)$, $y_{R,j}$ is the single-halo signal in the j th radial bin centred on the “right” LRG at $(+1, 0)$, and $p = p(X, Y)$ is a pixel on the map. When performing the fit, we choose radial bins of size $\Delta r = 0.02$, and we weight the map pixels uniformly. To avoid biasing the profiles with non-circular filament signal, we exclude the central region $-1 < X < +1$ and $-2 < Y < +2$ from the fit. Figure 3 shows the resulting best-fit profiles for the LRG halos.

Figure 4 shows the residual y map after subtracting the best-fit circular profiles shown in Figure 3 (note the change in colour scale from Figures 3 and 4). The bright halo signals appear to be cleanly subtracted, while a residual signal between the LRGs is clearly visible. The lower panels of Figure 4 show the residual signal in horizontal ($Y = 0$) and vertical ($X = 0$) slices through the

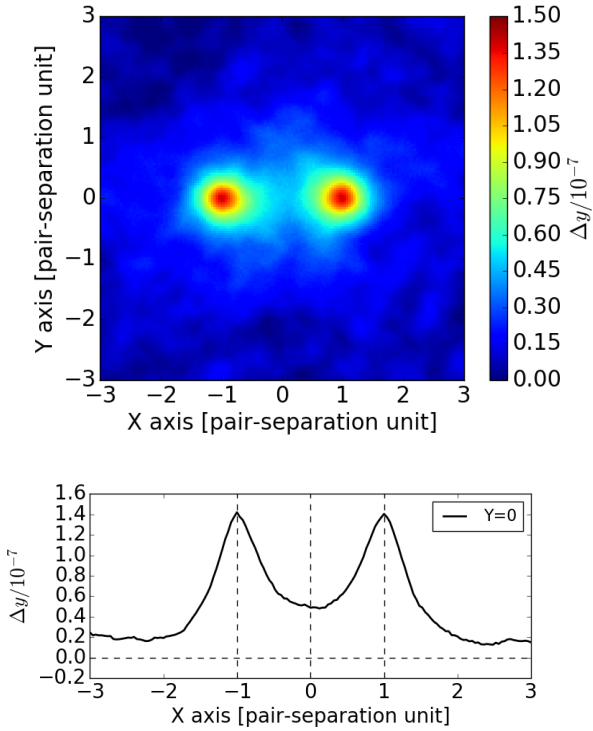


Figure 2. *Top:* The average *Planck* y map stacked against 262,864 LRG pairs in a coordinate system where one LRG is located at $(X, Y) = (-1, 0)$ and the other is at $(X, Y) = (+1, 0)$. The square region, $-3 < X, Y < +3$, comprises 151×151 pixels. *Bottom:* The corresponding y signal along the X axis.

map. The shape of the signal is consistent with an elongated filamentary structure connecting average pairs of central LRGs. The mean residual signal in the central region, $-0.8 < X < +0.8$ and $-0.2 < Y < +0.2$, is found to be $\Delta y = 1.31 \times 10^{-8}$.

3.3 Null tests and error estimates

To assess the reality of the residual signal and estimate its uncertainty, we perform two types of Monte Carlo-based null tests. In the first test, we rotate the centre of each LRG pair by a random angle in galactic longitude (while keeping the galactic latitude fixed, in case there is a systematic galactic background signal). We then stack the y map against the set of rotated LRG pairs, and we repeat this stacking of the full catalog 1000 times to determine the *rms* fluctuations in the background (and foreground) sky. Figure 5 shows one of the 1000 rotated, stacked y maps: the map has no discernible structure. We can use this ensemble of maps to estimate the uncertainty of the filament signal quoted above. Taking the same region used before ($-0.8 < X < +0.8$ and $-0.2 < Y < +0.2$), we find that the ensemble of null maps has a mean and standard deviation of $\Delta y = (-0.03 \pm 0.24) \times 10^{-8}$ in Figure 7. Since the average signal in this null test is consistent with zero, we cautiously infer that our estimator is unbiased, however, we present another test in the following.

The second null test is to stack the y map against “pseudo-pairs” of LRGs: that is, pairs of objects that satisfy the transverse separation criterion, but which have a large separation along the radial direction. Such pairs are not expected to be connected by filamentary gas. We generate a pseudo-pair catalog as follows: for

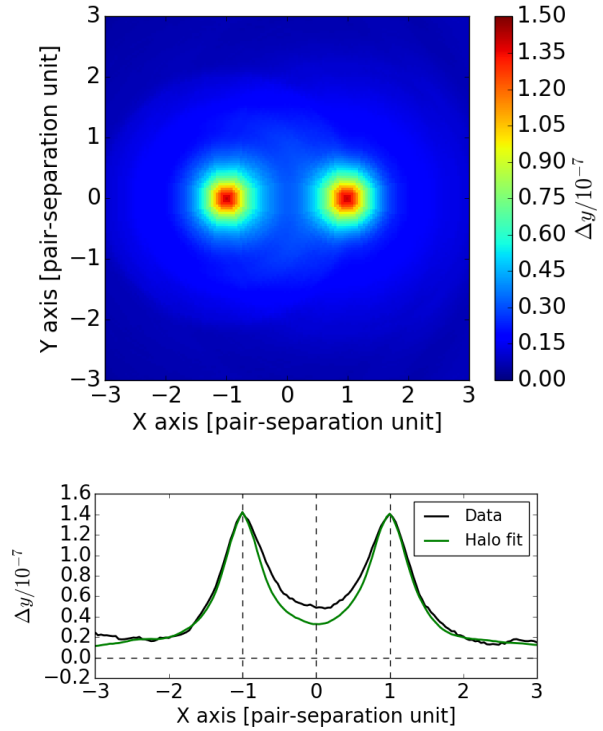


Figure 3. *Top:* The best-fit circular halo profiles fit to the map in Figure 2. *Bottom:* The best-fit radial profile of the left and right halos shown above.

each pair in the original catalog, we pick one of the two members at random, then pick a new partner LRG that is located within $6\text{--}10 h^{-1}\text{Mpc}$ of it in the transverse direction, but which is *more* than $30 h^{-1}\text{Mpc}$ away in the radial direction. We select the same number of pairs meeting this criterion as in default LRG pair catalog, so that the stacked image is of approximately the same depth. We repeat this selection 1000 times to generate an ensemble of pseudo-pair catalogs.

The top panel of Figure 6 shows an average y maps stacked against one of the pseudo pair catalog realizations. This map is similar to the genuine pair-stacked map shown in Figure 2, but with less apparent signal between the LRGs. We perform the same single-halo model fit described above and subtract it from the map with the result is shown in the middle panel of Figure 6. As with the rotated null test above, this map shows no discernible structure. To generate statistics, we repeat this test 1000 times: we find that the ensemble of null maps has a mean and standard deviation of $\Delta y = (0.00 \pm 0.25) \times 10^{-8}$ in Figure 7, virtually the same as with the rotated ensemble. We adopt this standard deviation as the final uncertainty of the mean filament signal due to instrument noise, sky noise (i.e., cosmic variance and foreground rejection errors), and halo subtraction errors.

4 INTERPRETATION

4.1 Systematic errors

Some systematic effects that might enhance or diminish the tSZ signal in the filaments may exist. For example, in our analysis, although we assume that the average single-halo contribution is circularly symmetric about each LRG, one might speculate that the

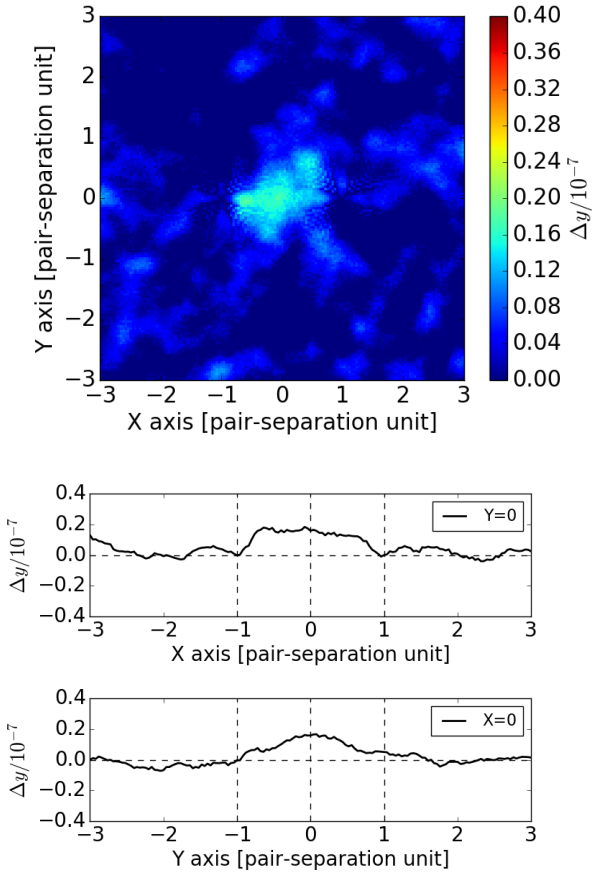


Figure 4. *Top:* The residual y-map after the best-fit radial halo signals are subtracted. *Bottom:* The residual tSZ signal along the X and Y axes.

signal we detect between nearby LRG pairs is a result of tidal effects, in which single-object halos are elongated along the line joining the two objects. However, considering that the $\sim 260,000$ LRG pairs are made from $\sim 220,000$ LRGs and each LRG has roughly 2 pairs (One is aligned between our LRG pairs and the other is not aligned), the direction of the elongation is not obvious. While tidal effects must be present at some level, if they were the dominant explanation for the residual signal we see, we would expect the elongated halo structure to extend in *both* directions along the line joining the objects. The fact that we see no significant excess signal outside the average pair suggests that tidal effects are not significant.

On the other hand, there are possible systematic effects that might lower the tSZ signal in the filaments. For example, some of the LRG pairs are not connected by filaments, or some of the filaments may not be straight but curved. However, in a study of N -body simulations, Colberg et al. (2005) found that cluster pairs with separations $< 5h^{-1}$ Mpc are always connected by dark matter filaments, mostly straight filaments. Further, they found filaments connecting $\sim 85\%$ of pairs separated by $5\text{--}10h^{-1}$ Mpc and $\sim 70\%$ of pairs separated by $10\text{--}15h^{-1}$ Mpc. This effect would lower the average y-value in the stacked filament and/or broaden the shape at some level, but the simulation study implies that most LRG pairs should be connected by dark matter (and presumably gas) filaments, and that dilution is unlikely to be significant.

In addition, there may be effects from asymmetric feature out-

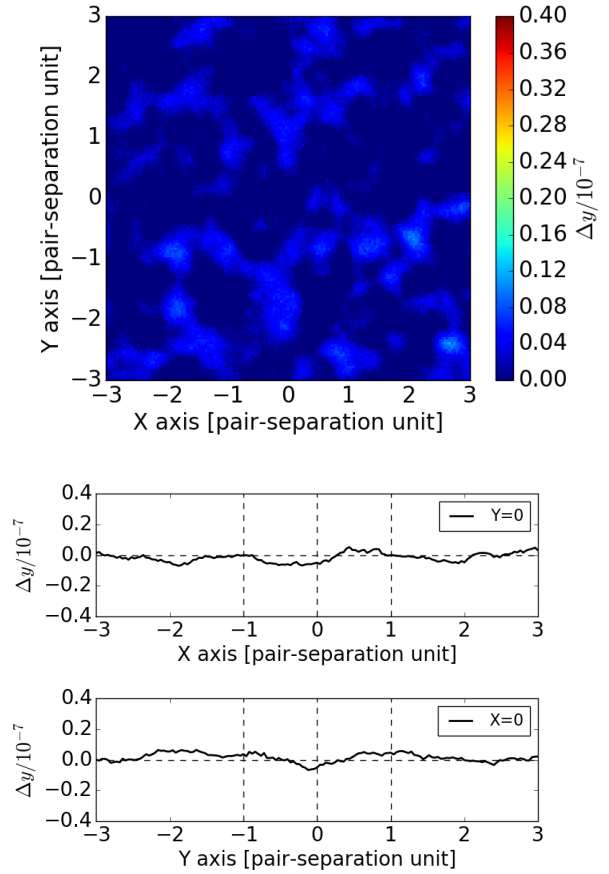


Figure 5. *Top:* A sample null map obtained by stacking the y map against the LRG pairs that were rotated in galactic longitude by random amounts. *Bottom:* The tSZ signal along the X and Y axes of the y map shown above.

side halos, due to the filaments extending out to different direction other than between our LRG pairs. We estimate the effect assuming circularly symmetric distribution of unaligned filaments around the halos. The aligned-filaments between the LRG's occupy roughly 10% with $\Delta y \sim 1.0 \times 10^{-8}$ region around a circular halo, so one unaligned filament makes only a few % extra excess on top of the circular halo profile and the effect should be negligible.

Furthermore, there might be an effect due to the *Planck* beam. We study the beam effect for the filaments using the BAHAMAS simulations. Using the smoothed y maps, the result is $\Delta y = 0.84 \times 10^{-8}$ in §5 and it is $\Delta y = 1.00 \times 10^{-8}$ with the unsmoothed y maps. With the study, we find that the beam dilutes the amplitude of y-value by $\sim 15\%$, although the mean separation angle between the LRGs is ~ 0.7 deg, therefore, the beam effect should not be significant in our study.

4.2 Unbound diffuse gas or bound gas in halos?

Is the signal we detect due to unbound diffuse gas outside of halos or bound gas in halos between the LRG pairs? To investigate this, we simulate a model y map using only bound gas in the SDSS DR12 LRGs with $10^{10}M_{\odot} < M_{*} < 10^{12}M_{\odot}$ and $0. < z < 0.8$ and compare the result with *Planck* y map. To make the single-halo model y map, we select “central” LRGs described in §2.1, which leaves $\sim 1,100,000$ LRGs, and estimate the halo masses of the

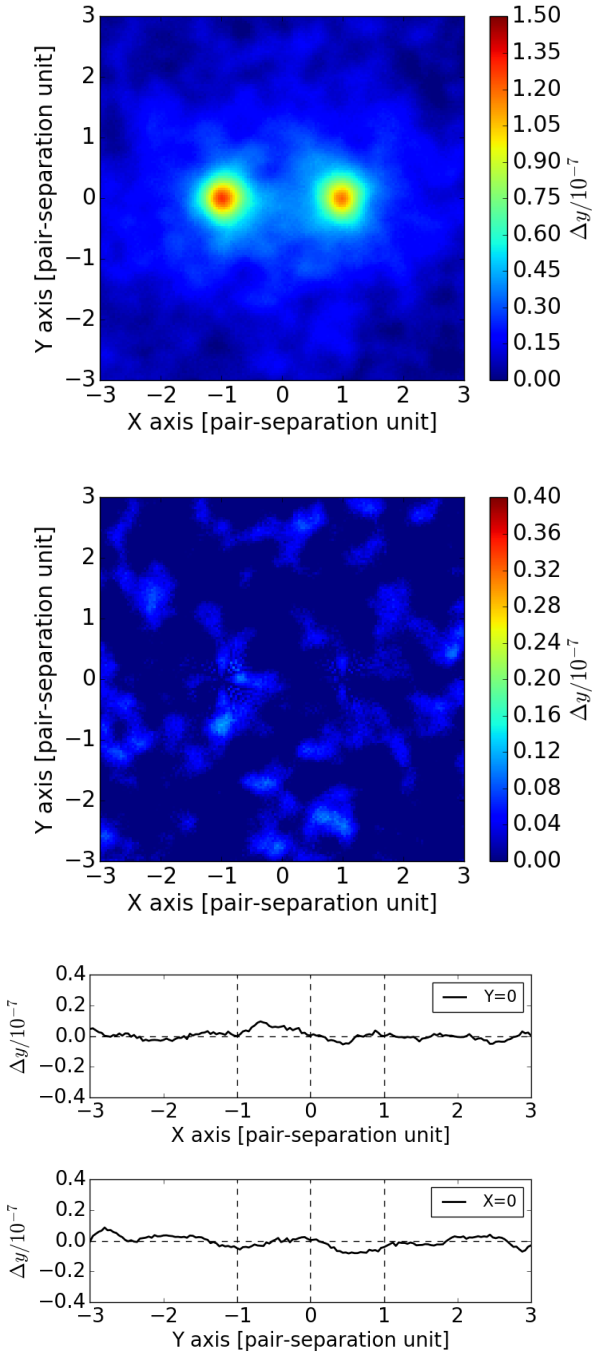


Figure 6. *Top:* An average y map stacked against a catalog of LRG pseudo-pairs (see text for a definition). *Middle:* The residual y map after subtracting the best-fit circular halos from the above map, using the same procedure that was applied to the genuine pair stack. *Bottom:* The tSZ signal along the X and Y axes of the residual map shown in the middle panel.

LRGs with the stellar-to-halo mass relation of [Coupon et al. \(2015\)](#), estimated in the CFHTLenS/VIPERS field by combining deep observations from the near-UV to the near-IR, supplemented by ~ 70 000 secure spectroscopic redshifts, and analyzing galaxy clustering, galaxy-galaxy lensing and the stellar mass function. Then we locate y profiles within the virial radius ($r < r_{200}$) of the LRG halos on the map using the universal pressure profile (UPP), which

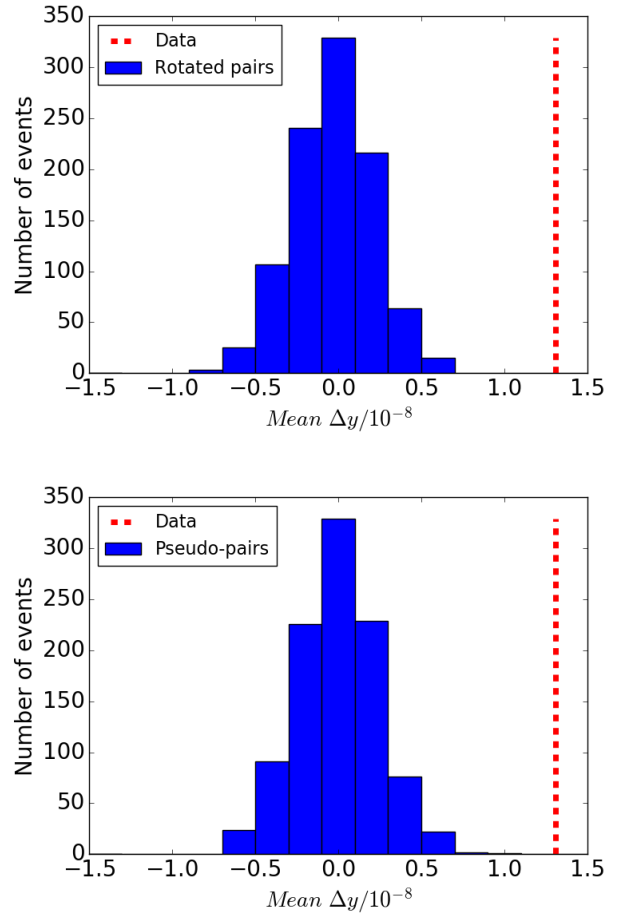


Figure 7. *Top:* The mean filament amplitude measured in 1000 randomly-rotated pair stacks. *Bottom:* The same statistic evaluated in 1000 pseudo-pair stacks. Both tests are consistent with zero residual signal. The mean filament amplitude measured in the data ($\Delta y = 1.31 \times 10^{-8}$) is indicated by red-dash line.

has an analytical formulation given by [Nagai et al. \(2007\)](#) for the generalised Navarro-Frenk-White (GNFW) profile ([Navarro et al. 1997](#)). For the parameters in the GNFW, we adopt the best-fit values of $[P_0, c_{500}, \gamma, \alpha, \beta] = [6.41, 1.81, 0.31, 1.33, 4.13]$, estimated using *Planck* tSZ and XMM-Newton X-ray data in [Planck Collaboration et al. \(2013a\)](#). For the model y map, we perform the same analysis. The peak y value of the LRG halos in Figure 8 is dimmer than the y map in Figure 2 since we only include the contribution within the virial radius of the LRG halos and in addition, no subhalos are included. After the circular halo subtraction, we obtain $\Delta y = 0.29 \times 10^{-8}$ from the bridge region. Moreover, we simulate a model y map including y profiles within $r < 3 \times r_{200}$ of the LRG halos and the result is $\Delta y = 0.36 \times 10^{-8}$. These results suggest that most of the y signal we detect between the LRGs should originate in unbound diffuse gas, although the contributions from other types of galaxies, less massive galaxies and galaxies in higher redshift should be present at some level.

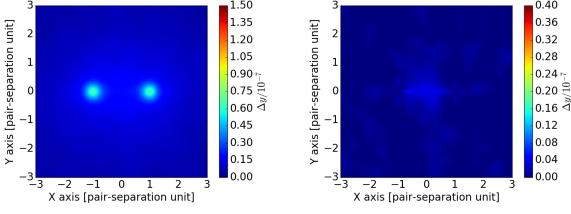


Figure 8. *Left:* The single-halo model y map described in the text is stacked against the same 262,864 LRG pairs as in the data analysis. *Right:* The residual model y map after subtracting the best-fit circular halos from the map at *left*, using the same procedure that was applied to the genuine pair stack.

4.3 Gas properties

We can estimate the physical conditions of the gas we detect by considering a simple, isothermal, cylindrical filament model of electron over-density with a density profile proportional to r_c/r , at redshift z . The Compton y parameter produced by the tSZ effect is given by

$$y = \frac{\sigma_T k_B}{m_e c^2} \int n_e T_e dl. \quad (2)$$

In general, the electron density at position \mathbf{x} may be expressed as

$$n_e(\mathbf{x}, z) = \bar{n}_e(z)(1 + \delta(\mathbf{x})), \quad (3)$$

where $\delta(\mathbf{x})$ is the density contrast, and $\bar{n}_e(z)$ is the mean electron density in the universe at redshift z ,

$$\bar{n}_e(z) = \frac{\rho_b(z)}{\mu_e m_p}, \quad (4)$$

where $\rho_b(z) = \rho_c \Omega_b (1+z)^3$ is the baryon density at redshift z , ρ_c is the present value of critical density in the universe, Ω_b is the baryon density in units of the critical density, $\mu_e = \frac{2}{1+\chi} \approx 1.14$ is the mean molecular weight per free electron for a cosmic hydrogen abundance of $\chi = 0.76$, and m_p is the mass of the proton.

We can express the profile in the Comptonisation parameter as a geometrical projection of a density profile with $n_e(r, z)$

$$y(r_\perp) = \frac{\sigma_T k_B T_e}{m_e c^2} \int_{r_\perp}^R \frac{2r n_e(r, z)}{\sqrt{r^2 - r_\perp^2}} dr, \quad (5)$$

where r_\perp is the tangential distance from the filament axis on the map and R is the cut-off radius of the filaments. Assuming negligible evolution of the filaments, and a constant over-density, δ_c , at the core, out to $z = 0.4$ (the maximum redshift in our LRG sample),

$$n_e(r = 0, z) = \frac{n_e(r = 0, z) \bar{n}_e(z)}{\bar{n}_e(z)} = \delta_c \bar{n}_e(0) (1+z)^3. \quad (6)$$

We consider three density profiles,

$$n_e(r) = \text{constant} \quad (r < r_c), \quad (7)$$

$$n_e(r) = \frac{n_e(0)}{\sqrt{1 + (r/r_c)^2}} \quad (r < 5r_c), \quad (8)$$

$$n_e(r) = \frac{n_e(0)}{1 + (r/r_c)^2} \quad (r < 5r_c), \quad (9)$$

where r_c is the core radius. To regularize the profiles, we adopt a cutoff radius of $5r_c$ for the second and third profile. Applying the profiles to the simulations, we find the best-fit density profile to follow (r_c/r) .

For this model, the predicted mean tSZ signal, $\overline{\Delta y}$, in the region $-0.8 < X < +0.8$, $-0.2 < Y < +0.2$, for the 262,864 filaments may be written as

$$\overline{\Delta y} = 4.9 \times 10^{-8} \times \left(\frac{\delta_c}{10} \right) \left(\frac{T_e}{10^7 \text{ K}} \right) \left(\frac{r_c}{0.5 h^{-1} \text{ Mpc}} \right). \quad (10)$$

Applying the observational constraint $\overline{\Delta y} = (1.31 \pm 0.25) \times 10^{-8}$, we have,

$$\delta_c \left(\frac{T_e}{10^7 \text{ K}} \right) \left(\frac{r_c}{0.5 h^{-1} \text{ Mpc}} \right) = 2.7 \pm 0.5. \quad (11)$$

Assuming the same temperature and morphology estimates from the simulations studied in §5 below apply to the observational data, the mean filament over-density between LRG pairs is $\delta \sim 3.2 \pm 0.7$. This suggests that the gas in the filaments between LRGs has a relatively low density.

5 COMPARISON WITH HYDRODYNAMIC SIMULATIONS

We compare our results to simulations. To do so, we analyze light cones from the BAHAMAS suite of simulations (§2.3) as we did the real data. For each cosmology, we construct simulated LRG pairs by selecting central galaxies with the same separation criteria as the real data. We invoke a stellar mass threshold such that the mean stellar mass of the sample matches the mean of the data. The resulting catalog has 242,669 pairs. Prior to stacking, we also convolve the simulated y map in each light cone with a 10 arcmin FWHM Gaussian kernel to match the *Planck* map. After stacking and radial halo subtraction, we find the residual tSZ signal between central galaxy pairs to be $\Delta y = (0.84 \pm 0.24) \times 10^{-8}$ with the *WMAP9* cosmology. The uncertainty is estimated by drawing 1000 bootstraps samples from among the 40 light cones. We have also analyzed the simulations based on the *Planck* 2013 cosmology and find $\Delta y = (1.14 \pm 0.33) \times 10^{-8}$. However, this model only has one realization of the initial conditions, instead of four, so it has a larger uncertainty than the *WMAP9* estimate. In conclusion, we find a slightly lower, but marginally consistent result from the simulations for both cosmologies.

The comparison of the simulations to the data is not entirely straightforward because of possible selection effects. In particular, the methods for estimating stellar mass in these two systems are different. The data estimates we use are based on the principal component method in [Chen et al. \(2012\)](#), which are, on average, ~ 0.2 dex higher than those based on spectro-photometric model fitting ([Maraston et al. 2013](#)). The simulation estimates we use are based on directly counting the baryonic mass within 30 kpc of a given central galaxy. As noted in §2.1, we adopt a stellar mass threshold of $10^{11.3} M_\odot$ for the data. In order to match the *mean* stellar mass of the simulation population, we must adopt a stellar mass threshold of $10^{11.2} M_\odot$. This procedure produces the same peak y values at the center of each mean halo: data and simulation. We believe this selection should produce comparable filament amplitudes.

In addition, we examine four independent realizations of the *WMAP9* cosmology and find that the mean residual tSZ signal between central galaxy pairs varies by a factor of ~ 5 , from $\Delta y = 0.26 \times 10^{-8}$ to 1.37×10^{-8} . This reflects the fact that cosmic variance is larger in the simulations than in the data due to their limited volume.

With the caveats noted above, we can use the simulations to

further probe the physical conditions in the observed filaments using the high-resolution simulated maps. In Figure 9, we separately examine the electron over-density and temperature in the stacked simulation data. For each light cone in our simulation box, we form optical depth and electron temperature maps,

$$\Delta\tau = \tau - \bar{\tau} \left(\text{with } \tau = \sigma_T \int n_e dl \right), \quad (12)$$

$$T_e = \frac{\Delta y}{\Delta\tau \times \frac{k_B}{m_e c^2}}, \quad (13)$$

where σ_T is the Thomson scattering cross section, k_B is the Boltzmann constant, m_e is the electron mass, c is the speed of light, n_e is the electron number density, T_e is the electron temperature, and the integral is taken along the radial direction. $\bar{\tau}$ is the mean value at the local background described in §3.1. We fit a variety of density profile models (§4.3) to the stacked τ map, and find the best-fit profile to follow (r_c/r) , where r is the perpendicular distance from the cylinder axis, and $r_c = 0.5 h^{-1} \text{Mpc}$, where r_c is the core radius of the density profile. Assuming this profile, the best-fit central over-density is $\delta = 1.5 \pm 0.4$ for WMAP9 cosmology. From the T_e map, the mean electron-density-weighted temperature of the electron gas in the filament region is found to be $(0.82 \pm 0.06) \times 10^7 \text{ K}$.

6 DISCUSSION

Other groups have studied filamentary gas in the large scale structure. We compare and contrast those results to ours as follows.

The *Planck* Team (Planck Collaboration et al. 2013b) studied the gas between the merging Abell clusters A399 and A401, which have a tangential separation of $3 h^{-1} \text{Mpc}$. Using a joint analysis of *Planck* tSZ data and ROSAT X-ray data, they estimate a gas temperature of $kT = 7.1 \pm 0.9 \text{ keV}$ ($T \sim 8.2 \times 10^7 \text{ K}$), and a central electron density of $n_e = (3.72 \pm 0.17) \times 10^{-4} \text{ cm}^{-3}$ ($\delta \sim 1500$). Assuming a filament diameter of 1.0 Mpc with a cylindrical shape, it corresponds to $y \sim 10^{-5}$. This high density and temperature may be because the filaments in merger systems have been shock-heated and compressed more than normal.

Using XMM-Newton observations, Werner et al. (2008) study the gas properties in a filament connecting the massive Abell clusters A222 and A223, at redshift $z \sim 0.21$. Assuming a separation of 15 Mpc , they find $kT = 0.91 \pm 0.25 \text{ keV}$ ($T \sim 1.1 \times 10^7 \text{ K}$) and $n_e = (3.4 \pm 1.3) \times 10^{-5} \text{ cm}^{-3}$ ($\delta \sim 150$). In addition, Eckert et al. (2015) find filamentary structures around the galaxy cluster Abell 2744, at $z \sim 0.3$, and estimate a gas temperature of $T \sim 10^7 \text{ K}$, and an over-density of $\delta \sim 200$ on scales of 8 Mpc . Assuming a filament diameter of 1.0 Mpc with a cylindrical shape, it corresponds to $y \sim 10^{-7}$, which is one order of magnitude higher than our result.

In a study with targets in our mass range, but using the CFHTLenS mass map, Epps & Hudson (2017) examined the weak lensing signal between pairs of SDSS-III/BOSS LRG's. They find a mass of $(1.6 \pm 0.3) \times 10^{13} M_\odot$ for a stacked filament region of $7.1 h^{-1} \text{Mpc}$ long and $2.5 h^{-1} \text{Mpc}$ wide. Assuming a uniform-density cylinder, they estimate $\delta \sim 4$ in the filaments, consistent with our result.

A simulation study, Colberg et al. (2005) examined 228 filaments between pairs of galaxy clusters in a ΛCDM N -body simulation produced by Kauffmann et al. (1999). They identify straight mass filaments longer than $5 h^{-1} \text{Mpc}$, normalize the length of each

filament to unity, and find the average density of matter contained within $2 h^{-1} \text{Mpc}$ of the (normalized) filament axis to be $\delta \sim 7$. This is somewhat higher than our estimate of $\delta = 3.2 \pm 0.7$, however, the following factors may compromise this comparison.

1) They select halos with masses larger than $10^{14} M_\odot$, whereas we select LRGs with the stellar masses larger than $10^{11.3} M_\odot$. According to the stellar mass / halo mass (SHM) relation used in Planck Collaboration et al. (2013c), this corresponds to halo masses with $M_{200} \sim (5 - 7) \times 10^{13} M_\odot$, and may include lower mass systems, given the scatter in the SHM relation. West et al. (1995) suggest that the masses of filaments are correlated with the masses of the halos associated with them. Thus, this selection of low-mass halo pairs can result in lower-mass filaments, and hence a lower tSZ signal.

2) The ΛCDM simulation tracks dark matter, whereas we analyze hydrodynamic simulations which include baryonic effects such as radiative cooling, star formation, SN feedback and AGN feedback. The baryonic gas in the filaments may not trace the dark matter faithfully.

3) They examine filaments between cluster pairs separated by $5 h^{-1}$ to $25 h^{-1} \text{Mpc}$, whereas we study smaller separations of 6 – $10 h^{-1} \text{Mpc}$.

7 CONCLUSION

Using the *Planck* Sunyaev-Zel'dovich (tSZ) map and the SDSS DR12 catalog of Luminous Red Galaxies (LRGs), we search for warm/hot gas filamentary gas between pairs of LRGs by stacking the y map on a grid aligned with the pairs. We detect a strong signal associated with the LRG host halos and subtract that using a best-fit, circularly symmetric model. We detect a statistically significant residual signal and draw the following conclusions.

- The residual tSZ signal in the region between LRG pairs is $\Delta y = (1.31 \pm 0.25) \times 10^{-8}$, with a 5.3σ significance. Assuming a simple, isothermal, cylindrical filament model of electron over-density with a radial density profile proportional to r_c/r (as determined from simulations), we constrain the physical parameters of the gas in the filaments to be

$$\delta_c \left(\frac{T_e}{10^7 \text{ K}} \right) \left(\frac{r_c}{0.5 h^{-1} \text{Mpc}} \right) = 2.7 \pm 0.5. \quad (14)$$

- We apply the same analysis to the BAHAMAS suite of cosmological hydrodynamic simulations (McCarthy et al. 2017). The results are marginally consistent, but the simulations predict a slightly lower mean tSZ signal of $\Delta y = (0.84 \pm 0.24) \times 10^{-8}$.

- Our result for the over-density in filaments is compatible with the results of Epps & Hudson (2017). They study the weak lensing signal between SDSS-III/BOSS LRG's and estimate $\delta \sim 4$, assuming a uniform-density, cylindrical filament model.

Our investigation can be extended with larger spectroscopic surveys such as extended BOSS (eBOSS) in SDSS-IV and the Dark Energy Spectroscopic Instrument (DESI). Their larger samples would improve the signal-to-noise and allow for a more detailed study of the physical conditions as a function of LRG properties, such as stellar mass and redshift. Large-area experiments with higher tSZ angular resolution, such as the Atacama Cosmology Telescope and the South Pole Telescope, would also help to ascertain the state of filament gas.

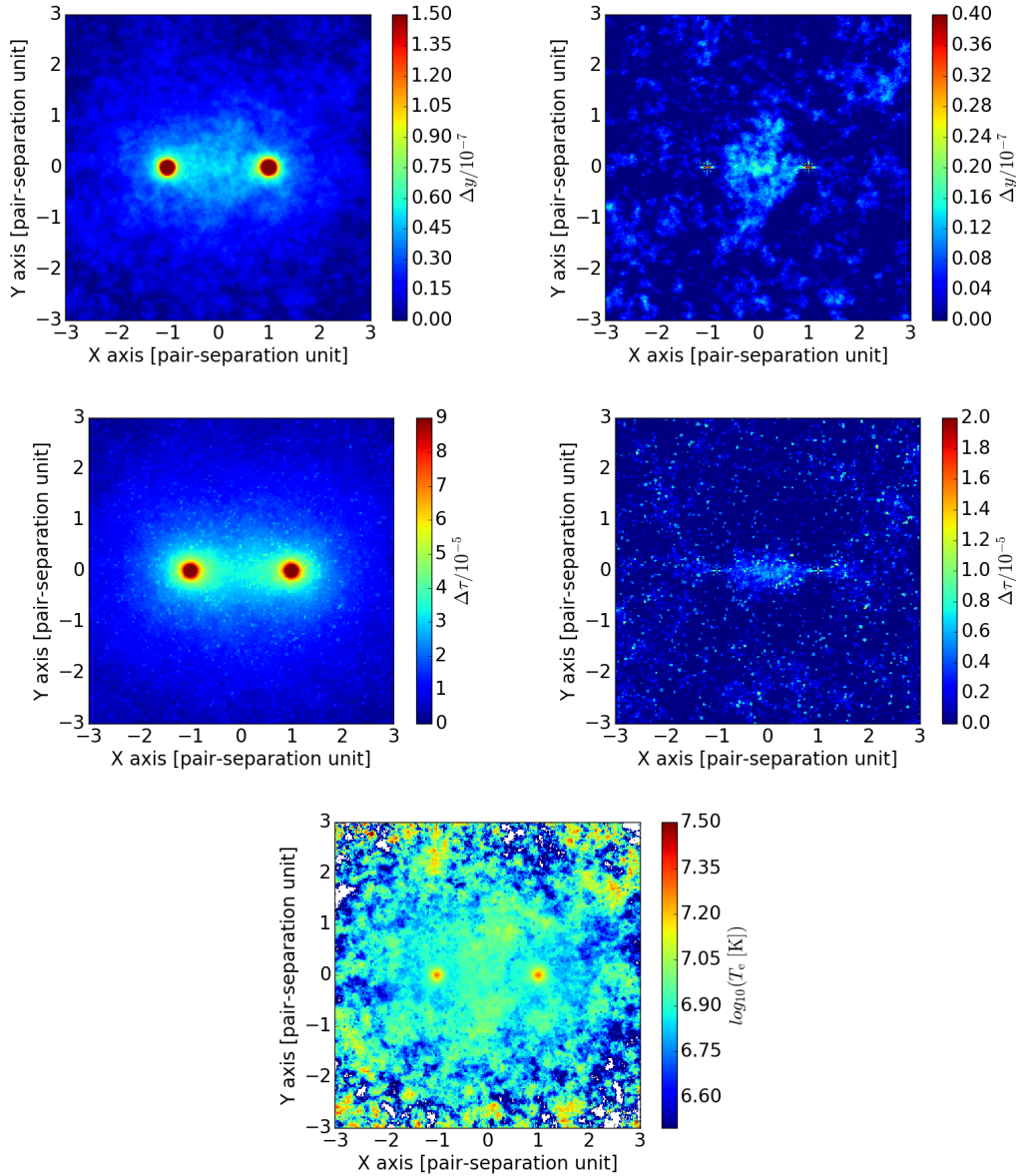


Figure 9. *Top left:* The stacked y map of the central galaxy pairs from the BAHAMAS simulations, at 10 arcsecond angular resolution. *Top right:* The same y map after the best-fit circular halos are subtracted. *Middle left:* The stacked τ map for the same pair sample as above. *Middle right:* The same τ map after circular halo subtraction. *Bottom:* The electron-density-weighted electron temperature map, T_e , on a \log_{10} scale.

ACKNOWLEDGEMENT

This research is funded by Canada's NSERC and CIFAR.

The data is based on observations obtained with Planck (<http://www.esa.int/Planck>), an ESA science mission with instruments and contributions directly funded by ESA Member States, NASA, and Canada, and observations obtained with SDSS-III, managed by the Astrophysical Research Consortium for the Participating Institutions of the SDSS-III Collaboration (<http://www.sdss3.org/>) funded by the Alfred P. Sloan Foundation, the Participating Institutions, the National Science Foundation, and the U.S. Department of Energy Office of Science.

The authors thank Joop Schaye for his contributions to the BAHAMAS project. This work used the DiRAC Data Centric system at Durham University, operated by the Institute

for Computational Cosmology on behalf of the STFC DiRAC HPC Facility (www.dirac.ac.uk). This equipment was funded by BIS National E-infrastructure capital grant ST/K00042X/1, STFC capital grants ST/H008519/1 and ST/K00087X/1, STFC DiRAC Operations grant ST/K003267/1 and Durham University. DiRAC is part of the National E-Infrastructure.

REFERENCES

- Alam S., et al., 2015, *ApJS*, **219**, 12
- Anderson L., et al., 2014, *MNRAS*, **441**, 24
- Atrio-Barandela F., Mücke J. P., 2006, *ApJ*, **643**, 1
- Atrio-Barandela F., Mücke J. P., Génova-Santos R., 2008, *ApJ*, **674**, L61

- Bruzual G., Charlot S., 2003, *MNRAS*, **344**, 1000
- Cen R., Ostriker J. P., 2006, *ApJ*, **650**, 560
- Chen Y.-M., et al., 2012, *MNRAS*, **421**, 314
- Clampitt J., Miyatake H., Jain B., Takada M., 2016, *MNRAS*, **457**, 2391
- Colberg J. M., Krughoff K. S., Connolly A. J., 2005, *MNRAS*, **359**, 272
- Coupon J., et al., 2015, *MNRAS*, **449**, 1352
- Eckert D., et al., 2015, *Nature*, **528**, 105
- Eisenstein D. J., et al., 2005, *ApJ*, **633**, 560
- Epps S. D., Hudson M. J., 2017, *MNRAS*, **468**, 2605
- Fukugita M., Peebles P. J. E., 2004, *ApJ*, **616**, 643
- Hill J. C., Spergel D. N., 2014, *J. Cosmology Astropart. Phys.*, **2**, 030
- Hinshaw G., et al., 2013, *ApJS*, **208**, 19
- Hojjati A., McCarthy I. G., Harnois-Deraps J., Ma Y.-Z., Van Waerbeke L., Hinshaw G., Le Brun A. M. C., 2015, *J. Cosmology Astropart. Phys.*, **10**, 047
- Hoshino H., et al., 2015, *MNRAS*, **452**, 998
- Kauffmann G., Colberg J. M., Diaferio A., White S. D. M., 1999, *MNRAS*, **303**, 188
- Kazin E. A., et al., 2010, *ApJ*, **710**, 1444
- Kroupa P., 2001, *MNRAS*, **322**, 231
- Le Brun A. M. C., McCarthy I. G., Schaye J., Ponman T. J., 2014, *MNRAS*, **441**, 1270
- Ma Y.-Z., Van Waerbeke L., Hinshaw G., Hojjati A., Scott D., Zuntz J., 2015, *J. Cosmology Astropart. Phys.*, **9**, 046
- Maraston C., et al., 2013, *MNRAS*, **435**, 2764
- McCarthy I. G., Le Brun A. M. C., Schaye J., Holder G. P., 2014, *MNRAS*, **440**, 3645
- McCarthy I. G., Schaye J., Bird S., Le Brun A. M. C., 2017, *MNRAS*, **465**, 2936
- Nagai D., Kravtsov A. V., Vikhlinin A., 2007, *ApJ*, **668**, 1
- Navarro J. F., Frenk C. S., White S. D. M., 1997, *ApJ*, **490**, 493
- Nicastro F., Mathur S., Elvis M., 2008, *Science*, **319**, 55
- Planck Collaboration et al., 2013a, *A&A*, **550**, A131
- Planck Collaboration et al., 2013b, *A&A*, **550**, A134
- Planck Collaboration et al., 2013c, *A&A*, **557**, A52
- Planck Collaboration et al., 2014, *A&A*, **571**, A1
- Planck Collaboration et al., 2016a, *A&A*, **594**, A1
- Planck Collaboration et al., 2016b, *A&A*, **594**, A22
- Prakash A., et al., 2016, *ApJS*, **224**, 34
- Rauch M., et al., 1997, *ApJ*, **489**, 7
- Reid B. A., Spergel D. N., 2009, *ApJ*, **698**, 143
- Schaye J., et al., 2010, *MNRAS*, **402**, 1536
- Shull J. M., Smith B. D., Danforth C. W., 2012, *ApJ*, **759**, 23
- Sunyaev R. A., Zeldovich Y. B., 1970, *Ap&SS*, **7**, 3
- Sunyaev R. A., Zeldovich Y. B., 1972, Comments on Astrophysics and Space Physics, **4**, 173
- Sunyaev R. A., Zeldovich I. B., 1980, *ARA&A*, **18**, 537
- Van Waerbeke L., Hinshaw G., Murray N., 2014, *Phys. Rev. D*, **89**, 023508
- Weinberg D. H., Miralda-Escudé J., Hernquist L., Katz N., 1997, *ApJ*, **490**, 564
- Werner N., Finoguenov A., Kaastra J. S., Simionescu A., Dietrich J. P., Vink J., Böhringer H., 2008, *A&A*, **482**, L29
- West M. J., Jones C., Forman W., 1995, *ApJ*, **451**, L5
- Yao Y., Shull J. M., Wang Q. D., Cash W., 2012, *ApJ*, **746**, 166
- Zeldovich Y. B., Sunyaev R. A., 1969, *Ap&SS*, **4**, 301
- van Daalen M. P., Schaye J., McCarthy I. G., Booth C. M., Dalla Vecchia C., 2014, *MNRAS*, **440**, 2997

This paper has been typeset from a \LaTeX file prepared by the author.